

# On the Role of Caustic in Solar Gravitational Lens Imaging

Igor Loutsenko

Laboratoire de Physique Mathématique,  
CRM, Université de Montréal  
e-mail: loutseni@crm.umontreal.ca

## Abstract

We consider scattering of electromagnetic waves from a distant point source by the gravitational field of the sun, taking the field oblateness due to the quadrupole moment of the sun into account. It turns out that effects of the field oblateness can play an important role in formation of images by the solar gravitational lens in sub-micrometer wavelength range of the electromagnetic spectrum.

## 1 Introduction

The idea of using the sun as a powerful telescope goes back to Eshleman [1]: The gravitational field of the sun acts as a spherical lens to magnify the intensity of radiation from distant objects along a semi-infinite focal line with the nearest point of observations being about 550AU (for a general introduction, see e.g. [3], [4], [5]). For example, the intensity from a distant point source of electromagnetic (EM) radiation at  $\lambda = 1\mu\text{m}$  wavelength can be pre-magnified by the sun gravitational lens up to  $\mu \approx 10^{11}$  times. Depending on observation device, the resolvable angle between two point sources at this wavelength could be as small as  $10^{-10}$  arcsec.

Recently, properties of the solar gravitational lens attracted attention both due to discovery of numerous exo-(and possibly earth-like) planets and the success of the Voyager-1 spacecraft, presently operating at about 140AU. Possibilities of mega-pixel imaging of such planets from the focal line of solar gravitational lens are now being discussed.

In the present work we consider effects of oblateness of the gravitational field and that of rotation of the sun on the diffraction pattern of the lens. Although the quadrupole moment of the sun is very small, effects of oblateness, nevertheless, turns out to be of a great importance: The focal line caustic unfolds and can have several hundred meters in cross section in the closest points of observation. Moreover, for wavelengths in a micrometer range, the diffraction pattern of the point source changes significantly and the maximum of the point spread function (PSF) can decrease up to about three orders of magnitude, depending on direction of observation and the distance between the sun and an observer.

We stress that the last statement concerns the maximal intensity magnification of a point source (maximum of PSF), and not the intensity magnification from realistic extended source. Since the

”focal blur” of a gravitational lens is comparable with the size of the whole image, there will be no significant difference in the magnifications for realistic objects. For instance, for visible light from exo-planets of interest, the intensity pre-magnification is about  $10^5$ - $10^6$  [5], in contrast to  $\mu \sim 10^{11}$  for a point source [4], [10], and it is determined mainly by the geometrical optics. The wave effects are noticeable on the scale comparable with the diffraction resolution of the gravitational lens, which is of order of  $10^{-10}$  arcsec in the case of the sun. This angle is far more smaller than apparent sizes of objects to be observed. As a consequence, even strong (of orders of magnitude) change of maximum of the PSF is invisible without a sophisticated fine scale de-convolution of images (the one to be developed and used for the prospective mega-pixel imaging of exo-planets). However, the geometrical optics effects due to the size of unfolding caustic become important at much rougher resolution of de-convolution (e.g. about hecto/kilo-pixels for exo-planets of interest).

Note, that effects of oblateness have been considered earlier in the literature. For instance, in [1] some heuristic considerations of these effects were presented. In the work [7] some estimates also were made that led to a conclusion that the oblateness of the sun has a negligible effect. This conclusion has been drawn from the computation of difference in deflection angles in the sun equatorial and polar planes, which is based on a heuristic model of the gravitational field of the sun <sup>1</sup>. Rigorous estimates of the deflection corrections due to the quadrupole moment of the sun have been done earlier, for instance, by Epstein and Shapiro [6]. The correct expression for the size of the aberration/caustic was derived by e.g. Eshleman et al in [2]. Our estimates are based on direct computations using methods of the uniform (caustic) expansions in the geometrical theory of diffraction, rather than on empirical approaches.

It is also worthy to note that despite of existence of numerous works considering gravitational lensing by oblate objects, detailed studies of the wave-optical aspects of the problem applied to the solar gravitational lens in the sub-micrometer diapason of the EM spectrum has been done mainly for the spherically symmetric case [8], [9], [10], [11].

This work is organized as follows: In the next section we introduce notations and consider geometrical optics of a spheroid gravitational lens of small oblateness. In the 3rd section we consider the wave effects and derive the point spread function in the form of a one-dimensional integral and make its numerical evaluation. Two limiting cases when this integral can be computed analytically, (the case of observations in directions close to the sun equatorial plane and the case of observations in directions close to the sun polar axis) are considered in the 4th section. Conclusions as well as suggestions for further studies are made in the last section. The main text of the paper is supplemented with an Appendix where we double-check our results with the help of well-known algorithms from the geometrical theory of diffraction.

## 2 Geometrical Optics Problem

We are interested in description of the diffraction pattern of an asymptotically plane EM wave scattered by the gravitational field of the sun. For this we first review the geometrical optics counterpart

---

<sup>1</sup>In [7], the model of two spheres of half of density offset by the distance comparable with that determined by oblateness is used. This leads to an underestimate in the corrections to deflections by about three orders of magnitude in comparison with e.g. computations made by Epstein and Shapiro [6]. The latter are based on the model with correctly estimated quadrupole moment. As a consequence, the transverse aberration was also underestimated by about three orders of magnitude in [7]. The correct expression for the size of the aberration/caustic was derived by e.g. Eshleman et al in [2].

of this problem: namely the deflection of initially parallel light rays coming from an infinitely distant point source.

A trajectory of light in the gravitational field of the sun can be found using post-Newtonian approximations for the null-geodesics of the post-Minkowskii metric element (see e.g. [12], [13], [16], [14], [15])

$$ds^2 = \left(1 + 2\frac{\Phi}{c^2}\right) (cdt)^2 - \left(1 - 2\frac{\Phi}{c^2}\right) d\vec{r}^2 - \frac{8}{c^2} (\vec{A} \cdot d\vec{r}) dt,$$

where  $\Phi$  is the scalar (Newtonian) gravitational potential and  $\vec{A}$  is the gravitomagnetic vector potential.

In the asymptotically Cartesian heliocentric coordinate system where parallel beams are incoming from  $z = -\infty$ , the post-Newtonian deflection angle  $\vec{\alpha}$ , which is the difference between the incoming and outgoing beam direction vectors, equals the gradient of the two-dimensional potential  $\Psi(x, y)$

$$\vec{\alpha} = \nabla \Psi, \quad \nabla = (\partial_x, \partial_y), \quad \Psi(x, y) = -\frac{2}{c^2} \int_{z_{\text{source}} \rightarrow -\infty}^Z \left( \Phi(x, y, z) - \frac{2}{c} A_z(x, y, z) \right) dz, \quad (1)$$

where  $Z$  is the  $z$ -coordinate of an observer. For a compact lens, a combined contribution to  $\Psi$  from the dipole terms of  $\Phi$  and  $\vec{A}$  can be cancelled by a translation. Since the gravitomagnetic field of the sun, produced by its rotation, is a dipole field, without loss of generality we can set  $\vec{A} = 0$  (for more details see eg [16]).

When  $Z > 0, Z \gg r_g$ , where  $r_g \approx 3 \times 10^3 \text{m}$  is the gravitational radius of the sun, one can apply the thin lens approximation which leads to the following picture (see Figure 1): a light ray is incoming from  $z = -\infty$  and hitting the  $z = 0$  "lens plane" at  $(x, y)$ . At this plane it is deflected by the angle (1). Then, it follows that the outgoing ray intersects the observer plane  $z = Z > 0$  at the point whose position  $(X, Y)$  is determined by the extremum of the Fermat potential  $S$  ("lens equation"):

$$\partial_x S = 0, \quad \partial_y S = 0, \quad S = \frac{(X - x)^2 + (Y - y)^2}{2Z} - \Psi(x, y). \quad (2)$$

This equation is a manifestation of the Fermat principle for the beam delay time  $S/c + T(Z)$ .

The exterior Newtonian potential of the sun can be approximated by that of the quadrupole

$$\Phi(\vec{r}) = -\frac{r_g c^2}{2r} \left[ 1 - \frac{I_2}{2} \left( \frac{R_0}{r} \right)^2 \left( \frac{3(\vec{n} \cdot \vec{r})^2}{r^2} - 1 \right) \right], \quad (3)$$

where  $\vec{n}$  is a unit vector in the direction of the polar axis of the sun,  $R_0 \approx 7 \times 10^8 \text{m}$  is the sun radius and  $I_2 \approx 2 \times 10^{-7}$  is its dimensionless quadrupole moment.

Without loss of generality we select the coordinate system where

$$\vec{n} = (0, \sin \beta, \cos \beta) \quad (4)$$

with  $\beta$  being the angle between the polar axis of the sun and the incoming from  $z = -\infty$  beams (see Figure 1).

Introducing the polar coordinates  $(r_\perp, \phi)$  in the lens  $z = 0$ -plane

$$x = r_\perp \cos \phi, \quad y = r_\perp \sin \phi, \quad r = \sqrt{r_\perp^2 + z^2}$$

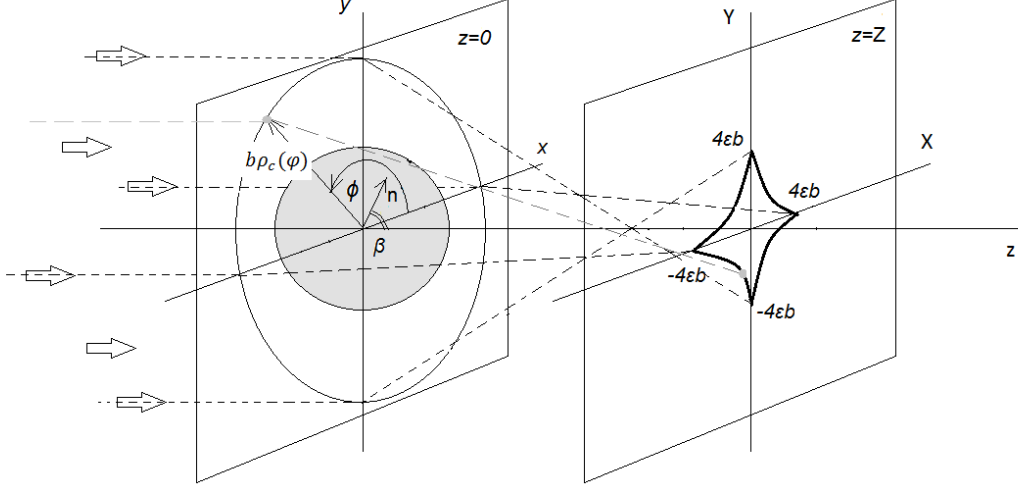


Figure 1: Diagram of the geometrical optics problem. Section of the caustic surface by the observer  $z = Z$  plane ( $X, Y$ -plane) is schematically shown on the right, while the corresponding critical line in the lens  $z = 0$  plane ( $x, y$ -plane) is schematically shown on the left.

and taking (1), (3) and the fact that  $Z \gg r_g$  into account we get <sup>2</sup> the two-dimensional potential  $\Psi$

$$\Psi = 2r_g \left( \log \frac{r_{\perp}}{r_g} - \frac{I_2 R_0^2 \sin^2 \beta}{2r_{\perp}^2} \cos 2\phi \right) + \text{const.} \quad (5)$$

In order not to carry numerous constants through the computations, we re-scale both the lens plane and the observer plane lengths with the scaling length parameter <sup>3</sup>  $b$

$$b \equiv \sqrt{2r_g Z}. \quad (6)$$

The new dimensionless polar coordinates  $(\rho, \phi)$  in the lens plane and the dimensionless Cartesian coordinates  $(\xi, \eta)$  in the observer plane then read

$$r_{\perp} = b\rho, \quad (x, y) = (b\rho \cos \phi, b\rho \sin \phi), \quad (X, Y) = (b\xi, b\eta). \quad (7)$$

In these coordinates

$$\Psi = 2r_g \psi, \quad \psi = \log(\rho) - \frac{\epsilon}{\rho^2} \cos 2\phi, \quad (8)$$

where

$$\epsilon = \frac{I_2 R_0^2 \sin^2 \beta}{4r_g Z} = \frac{I_2 R_0^2 \sin^2 \beta}{2b^2}. \quad (9)$$

In the case of the sun  $\epsilon \leq$  about  $10^{-7}$ . The small parameter  $\epsilon$  is maximal when  $\beta = \pi/2$ , i.e. when the source is placed in the sun equatorial plane. It decreases as the source is displaced towards the

<sup>2</sup> For details of this simple computation one can also refer to e.g. [15].

<sup>3</sup> We would like to stress that  $b$  is not an impact parameter. The latter will be introduced further.

sun polar axis, on which it vanishes (at  $\beta = 0$ ): The light radiated by a source from the polar axis is deflected as if the sun were spherically symmetric. So, we will refer to the both situations of  $I_2 = 0$  and  $\beta = 0$  as the "spherically symmetric", "degenerate" or the "monopole" case. The parameter  $\epsilon$  also decreases when the observer plane moves away from the sun (i.e. as  $Z$  increases).

It follows from (2,7, 8) that coordinates  $(\rho, \phi)$  of the images of the point  $(\xi, \eta)$  are solutions of the lens equation

$$\xi + i\eta = \left(\rho - \frac{1}{\rho}\right) e^{i\phi} - \frac{2\epsilon}{\rho^3} e^{3i\phi}. \quad (10)$$

We recall that the solution of this equation gives the "impact parameter"  $b\rho(\xi, \eta; \epsilon)$  and the corresponding polar angle  $\phi(\xi, \eta; \epsilon)$  in the lens plane for the ray(s) arriving to the observer plane at  $X = b\xi, Y = b\eta$ . Both scaling factor  $b$  and a small parameter  $\epsilon$  depend on distance  $Z$  between the planes.

In the geometrical optics, the inverse intensity magnification equals the ratio of the corresponding surface elements on the observer and the lens planes (the Jacobian of transformation (10) or the Hessian of the Fermat potential  $S$ )

$$\mu^{-1} = \left| \frac{\partial(X, Y)}{\partial(x, y)} \right| = \frac{1}{\rho} \left| \frac{\partial(\xi, \eta)}{\partial(\rho, \phi)} \right| = 1 - \frac{1}{\rho^4} - \frac{12\epsilon \cos 2\phi}{\rho^6} + \mathcal{O}(\epsilon^2). \quad (11)$$

The magnification  $\mu$  diverges at the critical line

$$\rho = \rho_c(\phi) = 1 + 3\epsilon \cos 2\phi + \mathcal{O}(\epsilon^2) \quad (12)$$

or, according to (10), at the astroid (tetracuspid) caustic <sup>4</sup> in the observer plane

$$(\xi, \eta) = (\xi_c(\phi), \eta_c(\phi)) = 4\epsilon(\cos^3 \phi, -\sin^3 \phi). \quad (13)$$

Here we recall the standard procedure of solving the lens equation (10). When the deviation of the observer from the  $z$ -axis is much smaller than  $b$ , i.e. when  $\xi \ll 1$  and  $\eta \ll 1$ , we have

$$\rho = 1 + \delta, \quad \delta \ll 1.$$

Then, from (10) it follows that  $\xi + i\eta = 2\delta e^{i\phi} - 2\epsilon e^{3i\phi}$ . Eliminating  $\delta$  from the last expression we get

$$\xi \sin \phi - \eta \cos \phi = 2\epsilon \sin 2\phi. \quad (14)$$

The solutions  $\phi$  of (14) are the "Einstein ring" coordinates of images of the point  $(\xi, \eta)$ . It is not difficult to see that those are angles between the  $\xi$ -axis and the tangents to the astroid (13) drawn from the point  $(\xi, \eta)$  (see Figure 2). When the point  $(\xi, \eta)$  is inside the astroid, equation (14) has four solutions. Otherwise it has two solutions. The magnification of the  $j$ th image  $\mu_j$  is inversely proportional to the distance from the observer to the corresponding tangency point on astroid (see also Appendix 1).

In the  $\epsilon = 0$  case the lens equation has two solutions when  $\xi^2 + \eta^2 \neq 0$  or infinite number of solutions forming a unit circle when  $\xi = \eta = 0$ . Since the number of solutions does not exceed four in the non-degenerate case, the image of a small source never forms the ring if  $\epsilon \neq 0$  (see Figure 2).

---

<sup>4</sup>According to the recent data the dimensionless octopole moment of the sun  $\sim 10^{-9}$ . Since  $\epsilon$  is at most  $\approx 10^{-7}$ , the caustic cross-section can be considered as a pure astroid for our purposes.

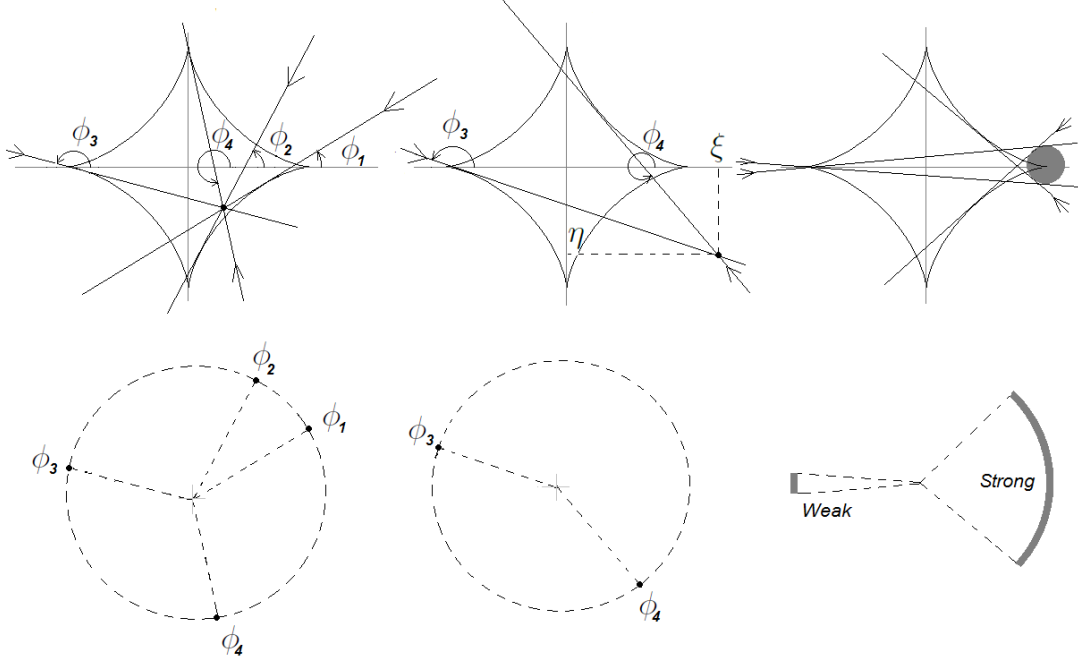


Figure 2: Top: Observer plane. Bottom: Lens plane. Left: Four point images of a point source viewed by an observer from an interior of the astroid. Center: Observer is outside the astroid (two point images). Right: Spans of the strong and weak ("limb") images of a small disc source viewed by an observer near the cusp. Maximal angular span of the "strong limb" is approximately proportional to the cubic root of the ratio between the size of the heliocentric projection of the source to the observer plane and the size of the astroid. Arrows on the tangents indicate directions of coming rays.

Returning to the  $\epsilon = 0$  case we note that the caustic (13) degenerates to the focal line  $\xi = 0, \eta = 0$  and the deflected beams converge towards the  $z$ -axis at the "Einstein" angles <sup>5</sup>  $|\alpha| = \alpha_E(Z)$

$$\alpha_E(Z) = \sqrt{\frac{2r_g}{Z}}. \quad (15)$$

The "on-axis" observer "sees" the whole critical line. In other words, the rays are coming from the circle of radius  $b$  in the lens plane towards an observer at  $X = Y = 0$  in the  $z = Z$  plane. Therefore,  $b > R_0$ , where  $R_0$  is the sun radius. The distance from the sun to the closest focal point is determined by the condition  $b = R_0$  and equals  $Z_{\min} = R_0^2/(2r_g) \approx 550$  AU.

In the wave optics, the maximal spatial resolution of the spherical lens in the neighborhood of the focal line is restricted by the radius of diffraction (radius of the Airy disc), which is of order  $\lambda/\alpha_E$ , where  $\lambda$  is the light wavelength [8],[9],[10], [11]: The circularly symmetric diffraction pattern of a point source oscillates in the radial direction and its intensity reaches maximum at the  $z$ -axis. The spatial scale of the oscillations is of order of the diffraction radius. For  $\lambda = 1\mu\text{m}$ , at the position of the closest observation  $Z \approx 550\text{AU}$ , this radius is about decimeters.

On the other hand, from eqs.(6, 9, 13) it follows that at the same conditions the non-spherical model produces an astroid caustic of the diameter  $4I_2R_0\sin^2(\beta)$ , which reaches up to  $\approx 5.6 \times 10^2$  meters when  $\beta \rightarrow \pi/2$ . Thus, effects of oblateness clearly lead to significant changes of the diffraction pattern of the point source when it moves from the sun polar axis to the equatorial plane. Indeed, the maximum of magnification is now reached in a neighborhood of astroid, where the geometrical optics magnification diverges, thousands of diffraction radiuses away from the  $z$ -axis, which is now nonsingular.

We note that, as follows from (7, 9, 13), size of the astroid is proportional to  $Z^{-1/2}$ , i.e. the size varies slowly with the distance from the sun (For example, the maximal astroid diameter is about 400 meters at 1000AU).

Before going to the detailed wave optics computations in the next section, we present some heuristic arguments explaining significant difference in the maximal magnifications of the point source in the  $\beta = 0$  and  $\beta = \pi/2$  cases for wavelengths of the interest: In the  $\epsilon = 0$  case (spherical lens) the lens plane image produced by a small distant source consists either of one single ring or two opposite arc-shaped "limbs" (one limb inside and another outside the critical curve  $\rho = \rho_c = 1$ ). Whether the image is a ring or limbs, as well as the size of limbs, depends on the source size and the observer position  $X, Y$  in the  $z = Z$  plane (the further away the observer is from the  $z$ -axis, the smaller are the limbs).

In difference from the symmetric case, in the case when the lens caustic is the astroid (13) the image of a small source <sup>6</sup> never forms the whole ring (see Figure 2). Such an image consists of two to four disjoint small limbs, some of them being weak and some strong, depending on the observer position wrt caustic. When the source size goes to zero, the limbs become a set of (two to four) points. Considering the principal Fresnel zones around these points one can explain decrease of maximal magnification in the wave optics.

In more details: the above zones have form of "limbs", whose dimensions depend on the size of caustic  $\sim \epsilon b$ , on the diffraction radius  $\sim \lambda/\alpha_E$  and on a position of the observer: It is easy to see that the thickness (i.e. radial dimension) of the limbs is approximately the same in symmetric and

<sup>5</sup>For a beam grazing the edge of the sun  $\alpha_E \approx 0.85 \cdot 10^{-5}$  rad  $\approx 1.75$  arcsec.

<sup>6</sup>By "small" we mean the source whose heliocentric projection to the observer plane has dimensions which are orders of magnitude smaller than the size of astroid.

non-symmetric cases when  $\epsilon$  is small (see e.g. [2]). However, in the spherically symmetric case even a point source can produce a circular geometrical optics image, and the maximal zone spans the whole circle even if  $\lambda \rightarrow 0$  (thickness of maximal zone goes to zero while its angular span always equals  $2\pi$ ). In contrast to the symmetric case, in the  $\epsilon \neq 0$  case the geometrical optics image of a point is always a point and therefore the maximal principal Fresnel zone contracts to a point as  $\lambda \rightarrow 0$ . This leads to decrease of the maximal magnification in comparison with the symmetric case <sup>7</sup> (since the thicknesses of zones have practically the same dependence on  $\lambda$  when  $\epsilon$  is small).

### 3 Diffraction Optics and Gravitational PSF

The geometrical theory of diffraction provides algorithms for finding near-caustic intensity from its geometric optics asymptotics [13], [17]. For caustics of the type (13) the near-field is expressed through the Airy function for caustic folds (see e.g. [13], [12], [19]), and through the Pearcey integral near caustic cusps (see e.g. [17], [20]). In cases of focal lines the near-field is expressed through Bessel functions [17], [19].

Application of these algorithms to our problem is presented in the Appendix 1.

Below, we derive the gravitational point spread function (GPSF) as a single one-dimensional integral having all the above mentioned limits.

The change of polarisation angles of light in weak gravitomagnetic fields is of a post-post Newtonian order and can be neglected (see eg [14], [18] and references therein). The deflection angles are also small and space is asymptotically flat, so we can apply the scalar Huygens-Fresnel principle (Fresnel-Kirchhoff diffraction formula): In the thin lens, short wavelength approximation ( $Z \gg R_0 \gg r_g$ ,  $\lambda \ll r_g$ ) the diffraction field in vicinity of the  $z$  axis is a sum of contributions by spherical waves propagating from the lens plane  $z = 0$  with the phase delays corresponding to the sum of the gravitational and geometric delays. This total time delay equals  $S/c + T(Z)$ , where  $S$  is given in (2). Then, the complex amplitude of the electromagnetic (EM) field at the observer position equals (up to a  $Z$ -dependent phase factor)

$$u = \frac{k}{2\pi Z} \int e^{ikS} dx dy, \quad k = 2\pi/\lambda. \quad (16)$$

The magnification (GPSF) equals the square of the absolute value of  $u$

$$\mu = |u|^2.$$

For a detailed derivation and justification of the Fresnel-Kirchhoff diffraction integral (16) see e.g. [12] or [19]. In (16), the geometrical optics magnification (11) is recovered as  $\lim_{k \rightarrow \infty} |u|^2$ . When  $kr_g \gg 1$  and the point on the observer  $X, Y$ -plane is far away from caustic, the integral (16) can be expressed in a simple manner through the geometrical-optics data as (see e.g. [19], [12])

$$u = \sum_j \sqrt{|\mu_j|} e^{i(kS_j - \pi n_j/2)}. \quad (17)$$

---

<sup>7</sup> An estimate of the maximal magnification based on the evaluation of dimensions of the Fresnel zone "visible" from the cusp of the caustic (13) was presented in [2]. There, the angular span ("horizontal dimension" in terminology of [2]) of the maximal Fresnel zone was overestimated due to a heuristic assumption that the "horizontal dimension" of the zone extends up to the point where the difference in the curvature radii of the critical line (12) corresponding to the zone center and the zone edge equals the "vertical" dimension (i.e. thickness) of the zone.



Here the sum is taken over the number of images in the lens plane,  $\mu_j$  is the geometrical optics magnification of the  $j$ th image,  $S_j = S(x_j, y_j)$  is the extremal value of the Fermat potential (2) for the  $j$ th image and  $n_j = 0, 1, 2$  corresponds to  $x_j, y_j$  being the minimum, saddle and the maximum point respectively. The above approximation breaks down in the neighborhood of caustic, the case we are mainly interested in. So, one has to either evaluate (16) exactly or to apply suitable asymptotic methods.

Up to a common ( $X, Y, Z$ -dependent) phase factor

$$u(\xi, \eta) = \frac{q}{2\pi} \int_{R_0/b}^{\infty} \rho d\rho \int_0^{2\pi} d\phi e^{iqV}, \quad V = \frac{\rho^2}{2} - \rho(\xi \cos \phi + \eta \sin \phi) - \psi(\rho, \phi), \quad (18)$$

where  $q$  is the dimensionless wavenumber

$$q = 2kr_g = \frac{4\pi r_g}{\lambda}. \quad (19)$$

For  $\lambda = 10^{-6}\text{m}$ ,  $q \approx 3.7 \times 10^{10}$ .

The main purpose of this section is the direct numeric evaluation of the 2d integral (18). Before presenting the numerical results we would like to make several remarks:

**Remark 1:** It is worthy to note that in the  $\epsilon = 0$  case, the exact 2d integration in (18) is possible:

$$u = \frac{q}{2\pi} \int \rho d\rho \int_0^{2\pi} e^{iq\left[\frac{\rho^2}{2} - \log(\rho) - \rho(\xi \cos \phi + \eta \sin \phi)\right]} d\phi = q \int \rho d\rho e^{iq\left[\frac{\rho^2}{2} - \log(\rho)\right]} J_0\left(q\rho\sqrt{\xi^2 + \eta^2}\right), \quad (20)$$

where  $J_0$  is the zero-order Bessel function. After integration in  $\rho$  one can express  $\mu$  in terms of the confluent hypergeometric function (see e.g. [19])

$$\mu = |u|^2 = \frac{\pi q}{1 - e^{-\pi q}} \left| {}_1F_1\left(iq/2, 1; iq(\xi^2 + \eta^2)/2\right) \right|^2.$$

In the short-wavelength limit  $q \gg 1$  and when the argument  $iq(\xi^2 + \eta^2)/2$  of  ${}_1F_1$  is small, i.e.

$$\sqrt{\xi^2 + \eta^2} \ll \frac{1}{\sqrt{q}}, \quad (21)$$

the hypergeometric function  ${}_1F_1$  degenerates to the zero-order Bessel function (see e.g. [19], [11])

$$\mu = \pi q J_0^2\left(q\sqrt{\xi^2 + \eta^2}\right).$$

The maximum  $\mu = \mu_0$  of the GPSF is reached at the focal line  $\xi = \eta = 0$  and equals

$$\mu_0 = \pi q = \frac{4\pi^2 r_g}{\lambda}. \quad (22)$$

**Remark 2:** Condition (21) is, in fact, a condition of validity of the stationary phase integration at  $\rho = 1$  in the last integral in (20). Indeed, the stationary phase approximation can be applied in (20) when the width of the stationary phase region  $\delta\rho \sim 1/\sqrt{q}$  is much more smaller than the scale of oscillations of the Bessel function  $\delta\rho \sim 1/(q\sqrt{\xi^2 + \eta^2})$ , which leads to (21).

**Remark 3:** Condition (21) will be encountered in the next section, when a similar type of the stationary phase integration will be performed for the general case  $\epsilon \neq 0$ : As follows from (18), in the general situation <sup>8</sup>

$$u = q \int \rho e^{iq \left[ \frac{\rho^2}{2} - \log(\rho) \right]} F(\epsilon q / \rho^2, q \xi \rho, q \eta \rho) d\rho, \quad F(\chi, \kappa, \nu) = \frac{1}{2\pi} \int_0^{2\pi} e^{\chi \cos 2\phi - \kappa \cos \phi - \nu \sin \phi} d\phi.$$

Similarly to the  $\epsilon = 0$  case, the stationary phase integration can be performed at  $\rho = 1$  when all the arguments of  $F$  are much smaller than  $\sqrt{q}$ , i.e. when

$$\epsilon \ll \frac{1}{\sqrt{q}} \quad (23)$$

and (21) holds. This will be demonstrated in detail in the next section.

Consider now the general case, i.e. the one when (21) is not necessarily true. Below we will proceed with the main subject of the present section, estimating the 2d integral (18) numerically without any assumptions.

Since  $q \gg 1$  (e.g.  $q \approx 3.7 \times 10^{10}$  for  $\lambda = 10^{-6}m$ ) one can reduce (18) to a one-dimensional integral in  $\phi$  by the stationary-phase integration <sup>9</sup> in  $\rho$  at fixed  $\phi$ : The stationary phase integration in  $\rho$  produces a relative  $\mathcal{O}(1/q)$  error, which is negligible for wavelengths of interest.

First, one should find the "stationary phase line"  $\rho = \rho_s(\xi, \eta; \phi)$  such that

$$\left( \frac{\partial V}{\partial \rho} \right)_{\rho=\rho_s} = \rho_s - \frac{1}{\rho_s} - \xi \cos \phi - \eta \sin \phi - \frac{2\epsilon \cos 2\phi}{\rho_s^3} = 0. \quad (24)$$

Then, up to a common phase factor

$$u = \sqrt{\frac{q}{2\pi}} \int_0^{2\pi} \left( \frac{\partial^2 V}{\partial \rho^2} \right)_{\rho=\rho_s(\phi)}^{-1/2} \rho_s(\phi) \exp[iqV(\rho_s(\phi), \phi)] d\phi. \quad (25)$$

From (24) we obtain that up to  $\mathcal{O}(\epsilon^2)$

$$\rho_s(\xi, \eta; \phi) = \frac{\sqrt{4 + s^2} + s}{2} + \frac{8\epsilon \cos 2\phi}{(\sqrt{4 + s^2} + s)^2 \sqrt{4 + s^2}}, \quad s = \xi \cos \phi + \eta \sin \phi \quad (26)$$

Therefore the GPSF (intensity magnification) expresses through the one-dimensional integral in  $\phi$ :

$$\mu = |u|^2 = \pi q |F|^2, \quad (27)$$

where

$$F = \frac{1}{\sqrt{2\pi}} \int_0^{2\pi} \left( 1 + \frac{1}{\rho_s^2} + \frac{6\epsilon \cos 2\phi}{\rho_s^4} \right)^{-1/2} \rho_s \exp iq \left[ \frac{\rho_s^2}{2} - \log \rho_s - s \rho_s + \frac{\epsilon \cos 2\phi}{\rho_s^2} \right] d\phi \quad (28)$$

with  $s = s(\xi, \eta; \phi)$  and  $\rho_s = \rho_s(\xi, \eta; \phi)$  given in (26).

<sup>8</sup> $F$  degenerates to  $J_0$  in two special cases: 1)  $\chi = 0$ , (i.e.  $\epsilon = 0$ ) and 2)  $\kappa = \nu = 0$  (i.e.  $X = Y = 0$ ), see eq. (50).

<sup>9</sup>For  $q \gg 1$ ,  $\int e^{iqf(x)} x dx = x_s \sqrt{\frac{2\pi i}{q f''(x_s)}} e^{iqf(x_s)} \left( 1 + \mathcal{O}\left(\frac{1}{q}\right) \right)$ , where  $f'(x_s) = 0$

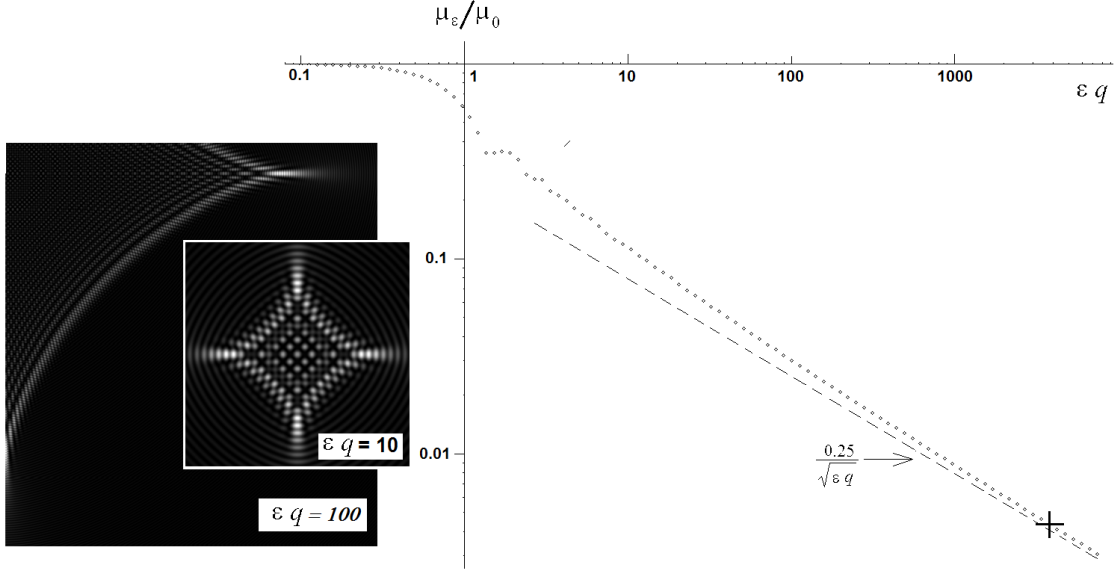


Figure 3: Left Figure: Normalized diffraction patterns for  $q = 3.7 \times 10^{10}$ ,  $\epsilon q = 10$  and  $\epsilon q = 100$ . The former image ( $q\epsilon = 10$ ) is  $3\times$  zoomed in wrt to the latter. Right Figure: The log – log plot of  $\mu_\epsilon/\mu_0$  as a function of  $\epsilon q$ . Numerical evaluation is shown by the point plot. High  $\epsilon q$  asymptotics (29) is shown by the dashed line. The point corresponding to observations in the equatorial plane of the sun at  $Z = 550$  AU and  $\lambda = 10^{-6}$ m is marked with a cross. At this point  $\epsilon q \approx 3.7 \times 10^3$  and  $\mu_\epsilon/\mu_0 \approx 4 \times 10^{-3}$ . Computations are performed for  $q = 3.7 \times 10^{10}$  that corresponds to  $\lambda \approx 10^{-6}$ m. Small parameter  $\epsilon$  varies from  $\epsilon \approx 2.7 \times 10^{-12}$  to  $\approx 2.0 \times 10^{-7}$ . Error of numeric integration  $\delta\mu_\epsilon/\mu_\epsilon$  does not exceed  $\approx 1$  percent.

The above integral can be particularly easy taken when  $\epsilon = 0$ ,  $\xi = \eta = 0$ , giving the value of  $\mu_0$ , obtained earlier (22). In the general case, the integral (28) should be taken numerically.

Now, we present results of the direct numerical computation of the GPSF (27,28): Figure 3 shows ratio of maximal intensity  $\mu_\epsilon$  at  $\epsilon \neq 0$  to that of the symmetric case  $\mu_0$  for different values of the parameter  $\chi = q\epsilon$ . The computation is performed for  $q = 3.7 \times 10^{10}$  which corresponds to  $\lambda = 1\mu m$ .

As seen from Figure 3 one naturally recovers the unit ratio for  $q\epsilon \rightarrow 0$

$$\frac{\mu_\epsilon}{\mu_0} \rightarrow 1, \quad q\epsilon \rightarrow 0.$$

On the other hand

$$\frac{\mu_\epsilon}{\mu_0} \approx \frac{0.25}{\sqrt{\epsilon q}} \quad (29)$$

when  $q\epsilon \gg 1$ . In this case four equal maxima of the intensity magnification are symmetrically situated on the  $X$ ,  $Y$  axes: two at the  $X$ -axis and another two at  $Y$ -axis in the caustic interior close to four cusp vertices  $(X, Y) = (\pm 4b\epsilon, 0)$ ,  $(X, Y) = (0, \pm 4b\epsilon)$ . When  $q\epsilon$  is large, the distance between the vertex and the neighboring maximum is proportional to  $\epsilon b / \sqrt{\epsilon q}$ .

The GPSF oscillates and the amplitude of oscillations grows as one moves towards the neighborhood of the caustic folds/cusps. The amplitude falls off similarly to the  $\epsilon = 0$  case and the pattern becomes more and more radially symmetric, as one moves far away from caustic in the exterior direction (which is in agreement with (17)).

When  $q\epsilon \rightarrow 0$ , the maxima move towards the center  $X = Y = 0$ , where they merge when  $\epsilon = 0$ . The diffraction pattern becomes circularly symmetric.

In the case of the sun at  $\lambda = 10^{-6}$  m, the parameter  $\chi = q\epsilon$  can be as large as  $\approx 3.7 \times 10^3$ . For these wavelengths the maximum magnification of the point source by solar gravitational lens can decrease up to several orders of magnitude when the source goes from the polar axis  $\beta = 0$  towards the equatorial plane  $\beta = \pi/2$  (see eq. (9)). An analytic explanation of the above numeric results is given below.

## 4 Diffraction Optics: Limiting Cases

For analytic description of the above numerical result we expand the argument of exponential in (28) in  $s$  and  $\epsilon$

$$F = \frac{1}{2\pi} \int_0^{2\pi} G e^{iqU} d\phi, \quad (30)$$

where, to the second order in  $s$  and  $\epsilon$

$$U = \frac{1}{2} - s + \epsilon \cos 2\phi - U_2, \quad U_2 = \left( \frac{s}{2} + \epsilon \cos 2\phi \right)^2 \quad (31)$$

and to the first order in  $s$ ,  $\epsilon$

$$G = 1 + \frac{3}{4}s. \quad (32)$$

We are interested in the short wavelength limit  $q \gg 1$  of (30). The  $U_2$ -term in (30, 31) can be neglected if  $q|U_2| \ll \pi$ . This condition holds when

$$|s| \ll \frac{2}{\sqrt{q}}, \quad \epsilon \ll \frac{1}{2\sqrt{q}}, \quad q \gg 1. \quad (33)$$

The above conditions have been already encountered in (21), (23).

Since  $|s| \ll 2/\sqrt{q}$  and  $q \gg 1$ , the  $s$ -term in (32) can be dropped. Therefore, provided (33) holds, up to the constant phase factor

$$F = \frac{1}{2\pi} \int_0^{2\pi} e^{iq(\epsilon \cos 2\phi - s)} d\phi = \frac{1}{2\pi} \int_0^{2\pi} e^{iq(\epsilon \cos 2\phi - \xi \cos \phi - \eta \sin \phi)} d\phi. \quad (34)$$

Rewritten in terms of  $X$  and  $Y$ , the condition imposed on  $s$  in (33) is  $|X \cos \phi + Y \sin \phi| \ll 2b/\sqrt{q}$ , i.e.

$$R \ll R_v = \frac{2b}{\sqrt{q}}, \quad R = \sqrt{X^2 + Y^2}, \quad (35)$$

where  $R$  is the distance between the observer and the  $z$ -axis. For  $\lambda \sim 10^{-6}\text{m}$  (i.e. for  $q \sim 10^{10} - 10^{11}$ ), the radius  $R_v$  is about 10 kilometers, while the maximum possible radius of the caustic is about 300 meters, so the above condition of validity of (34) clearly holds in the region of the interest <sup>10</sup>.

Therefore, to get the amplitude of EM field one can integrate over the circle  $\rho = 1$  in the lens plane provided (35) holds. This happens due to the fact that the "optical path"  $S$  is extremal <sup>11</sup> on the ray trajectories (see eq. (2)) and small deformations of the integration contour do not significantly change the "monopole part"  $S_0$  of  $S = S_0 + \epsilon S_1$  when (35) holds. Since the contour deformations are of order of  $\epsilon$ , the error in the quadrupole contribution  $\epsilon S_1$  is of order of  $\epsilon^2$ , which is also negligible. In other words, the width of the stationary phase integration region significantly exceeds the deviation of the integration contour  $\rho = \rho_s(\xi, \eta, \phi)$  from the unit circle when (35) is true.

Apart from the situation when (34, 35) overlaps with the approximation (17), analytical study of (34) can be performed for the three asymptotic cases:

1. The "degenerate" case  $q\epsilon \ll 1$ , i.e the case of observations in directions that are close to the sun polar axis  $\beta \ll \frac{b}{R_0} \sqrt{\frac{\lambda}{I_2 r_g}}$ . At  $Z \sim 550AU$  and  $\lambda \approx 10^{-6}$  this corresponds to  $\beta$ 's that are smaller than fraction of a degree.
2. The "strongly non-degenerate" case  $\chi = q\epsilon \gg 1$ , or equivalently  $\epsilon \gg \lambda/r_g$ . In this case the scale of the diffraction pattern is much more smaller than the transverse caustic size. According to (9, 6, 19)  $\beta \gg \frac{b}{R_0} \sqrt{\frac{\lambda}{I_2 r_g}} = \sqrt{2\lambda Z/(I_2 R_0^2)}$  for this asymptotics. At  $Z \sim 550AU$  and  $\lambda \approx 10^{-6}$ , this corresponds to the directions that are not close to the sun polar axis  $\beta \gg 5 \times 10^{-2}$ .
3. On-axis magnification, i.e. value of GPSF at  $X = Y = 0$  and an arbitrary  $\epsilon q$ .

1. We start with the first case, the spherical lens. When  $\epsilon = 0$ , (34) degenerates to the zero-order Bessel integral

$$F = \frac{1}{2\pi} \int_0^{2\pi} e^{-iq(\xi \cos \phi + \eta \sin \phi)} d\phi = J_0 \left( q \sqrt{\xi^2 + \eta^2} \right).$$

Since  $\xi = X/b$ ,  $\eta = Y/b$ ,  $q = 2kr_g = 4\pi r_g/\lambda$  and  $b = \sqrt{2r_g Z}$  (see eq.(6), (19)), from (27) we get

$$\mu = \pi q J_0^2(q \sqrt{\xi^2 + \eta^2}) = \frac{4\pi^2 r_g}{\lambda} J_0^2 \left( \frac{2\pi}{\lambda} \sqrt{\frac{2r_g}{Z}} R \right), \quad R = \sqrt{X^2 + Y^2}. \quad (36)$$

<sup>10</sup>The ratio of the radius  $R_v$  to the caustic radius  $4\epsilon b$  equals  $1/(2\epsilon\sqrt{q})$ , which leads to the condition  $\epsilon \ll 1/\sqrt{q}$ . Since for the sun  $\epsilon$  is at most about  $10^{-7}$ , this condition clearly holds in our case.

<sup>11</sup>The second tangential derivative of  $S$  also vanishes on the critical line.

Thus the  $\epsilon = 0$  limit, obtained alternatively in Section 3 by exact 2d integration of (18)) is recovered. This gives the well-known result [8],[9], [19], [10], [11] for the GPSF of the spherical lens.

The GPSF is circularly symmetric and reaches maximum  $\mu_0$  at  $R = 0$ . The radius of the Airy disc (i.e. "diffraction radius") and the spatial period of the radial Airy pattern is of order of  $\lambda/\alpha_E(Z)$ .

**2.** Let us now pass to the strongly non-degenerate case  $q\epsilon \gg 1$ . In this case the size of caustic  $\sim \epsilon b$  greatly exceeds the diffraction radius  $\sim \lambda/\alpha_E$ . First we consider the asymptotic of the GPSF in the cusp neighborhoods, where it reaches the maxima. For convenience we choose the cusp at  $X = 4\epsilon b, Y = 0$ , (i.e. at  $\xi = 4\epsilon, \eta = 0$ ).

We now introduce the cusp-related coordinates  $\tilde{\xi}, \tilde{\eta}$ , such that

$$\xi = \epsilon \left( 4 + \frac{2\tilde{\xi}}{\sqrt{2q\epsilon}} \right), \quad \eta = \frac{\sqrt{2}\epsilon\tilde{\eta}}{(2q\epsilon)^{3/4}},$$

and re-scale the integration angle  $\phi \rightarrow \varphi$

$$\phi = \frac{2^{1/4}\varphi}{(q\epsilon)^{1/4}}.$$

In these coordinates integral (34) rewrites as

$$F = \frac{1}{2\pi(q\epsilon/2)^{1/4}} \int_{-\pi(q\epsilon/2)^{1/4}}^{\pi(q\epsilon/2)^{1/4}} e^{i\tilde{V}(\varphi)} d\varphi, \quad (37)$$

where, modulo  $\varphi$ -independent terms,  $\tilde{V}$  has the following form

$$\tilde{V} = -\tilde{\eta}\varphi + \tilde{\xi}\varphi^2 + \varphi^4 + \tilde{V}_1, \quad \tilde{V}_1 = \frac{\sqrt{2}}{\sqrt{q\epsilon}} [\tilde{\xi}\varphi^4 P + \tilde{\eta}\varphi^3 Q + \varphi^6 H] \quad (38)$$

Here,  $P, Q, H$  are bounded functions ( $\max(|P|, |Q|, |H|) \leq 1/6$ ) of the single variable  $\phi = \frac{\varphi}{(q\epsilon/2)^{1/4}}$ ,  $\phi = -\pi.. \pi$ .

$$P = \frac{1 - \frac{\phi^2}{2} - \cos \phi}{\phi^4}, \quad Q = \frac{\phi - \sin \phi}{\phi^3}, \quad H = 2 \frac{\cos 2\phi - 4 \cos \phi + 3 - \frac{\phi^4}{2}}{\phi^6}, \quad \phi = -\pi.. \pi.$$

Since  $q\epsilon \gg 1$ , the  $\tilde{V}_1$  term in (38) can be neglected when

$$|\tilde{\xi}| \ll \sqrt{q\epsilon}, \quad |\tilde{\eta}| \ll \sqrt{q\epsilon}. \quad (39)$$

Then, provided the above conditions hold, from (37, 38) it follows that

$$F = \frac{1}{2\pi(q\epsilon/2)^{1/4}} \text{Pe}(\tilde{\xi}, \tilde{\nu}),$$

where  $\text{Pe}(x, y)$  is the Pearcey integral

$$\text{Pe}(x, y) = \int_{-\infty}^{\infty} e^{i(-y\varphi + x\varphi^2 + \varphi^4)} d\varphi. \quad (40)$$

It follows from (27) that in terms of unscaled deviation  $\tilde{X} = X - 4\epsilon b$ ,  $\tilde{Y} = Y$  from the cusp vertex the near-cusp GPSF equals

$$\mu = \frac{1}{4\pi} \sqrt{\frac{2q}{\epsilon}} \left| \text{Pe} \left( \frac{\tilde{X}}{2\epsilon b} (2\epsilon q)^{1/2}, \frac{\tilde{Y}}{\epsilon b} (2\epsilon^3 q^3)^{1/4} \right) \right|^2. \quad (41)$$

The domain of validity (39) of the above asymptotics rewrites in terms of the unscaled deviations from the cusp vertex as follows

$$|\tilde{X}| = |X - 4\epsilon b| \ll \epsilon b, \quad |\tilde{Y}| = |Y| \ll \frac{\epsilon b}{(q\epsilon)^{1/4}}. \quad (42)$$

We recall that the above conditions are in agreement with (35), since, as has been mentioned before, the "radius of validity" of (34) greatly exceeds maximal possible size of caustic when  $\epsilon \ll 1/\sqrt{q}$ .

The absolute value of the Pearcey integral  $|\text{Pe}(\tilde{\xi}, \tilde{\eta})|$  reaches maximum at  $\tilde{\xi} \approx -2.02$ ,  $\tilde{\eta} = 0$  which is inside the domain of validity (39) of eq. (41). The maximum of GPSF in the  $\epsilon q \gg 1$  limit then equals

$$\mu_\epsilon = \frac{1}{4\pi} \sqrt{\frac{2q}{\epsilon}} \max |\text{Pe}|^2 = \sqrt{\frac{r_g}{2\pi\lambda\epsilon}} \max |\text{Pe}|^2, \quad \max |\text{Pe}|^2 \approx 7.02.$$

Therefore the ratio of the maximum  $\mu_\epsilon$  to that of the spherically symmetric case  $\mu_0$  equals

$$\frac{\mu_\epsilon}{\mu_0} = \frac{\sqrt{2} \max |\text{Pe}|^2}{4\pi^2} \frac{1}{\sqrt{q\epsilon}} \approx \frac{0.25}{\sqrt{q\epsilon}}, \quad q\epsilon \gg 1. \quad (43)$$

The distance between point of maximum and the cusp vertex equals  $\approx 2.02\epsilon b/\sqrt{\epsilon q/2}$ . This confirms the numerical results of the Section 3.

In difference from the symmetric case, where the circular invariant diffraction pattern has radial oscillations, the near-cusp pattern in the  $q\epsilon \gg 1$  case has a complicated two-dimensional lattice-like structure (see Figures 3, 4). The latter transforms towards locally one dimensional structure of smaller intensity (48) as one moves along the caustic away from the cusp.

We now evaluate the GPSF in the vicinity of caustic folds (regular points of caustic) far from the cusps<sup>12</sup>.

It is convenient to introduce the caustic-linked coordinates  $\sigma, \theta$  (see Figure 5)

$$\xi = 4\epsilon \cos^3 \theta - \sigma \sin \theta, \quad \eta = -4\epsilon \sin^3 \theta + \sigma \cos \theta \quad (44)$$

with  $\sigma$  being the dimensionless length of the perpendicular from the point  $(\xi, \eta)$  to the caustic fold. According to (34), in these coordinates

$$F = \frac{1}{2\pi} \int_0^{2\pi} e^{iV} d\phi, \quad V = q\sigma \sin(\theta - \phi) + \epsilon q \left( \cos 2\phi + 4 \sin^3 \theta \sin \phi - 4 \cos^3 \theta \cos \phi \right). \quad (45)$$

Introducing new integration variable  $\varphi$  as well as making the change of  $\sigma$ :

$$\phi = \theta + \frac{\varphi}{(3q\epsilon \sin 2\theta)^{1/3}}, \quad \tilde{\sigma} = \frac{-\sigma q}{(3\epsilon q \sin 2\theta)^{1/3}},$$

---

<sup>12</sup>Description of diffraction pattern in a fold neighborhood is extensively presented in the literature on the gravitational lensing. For a review, see e.g. [12], [19]

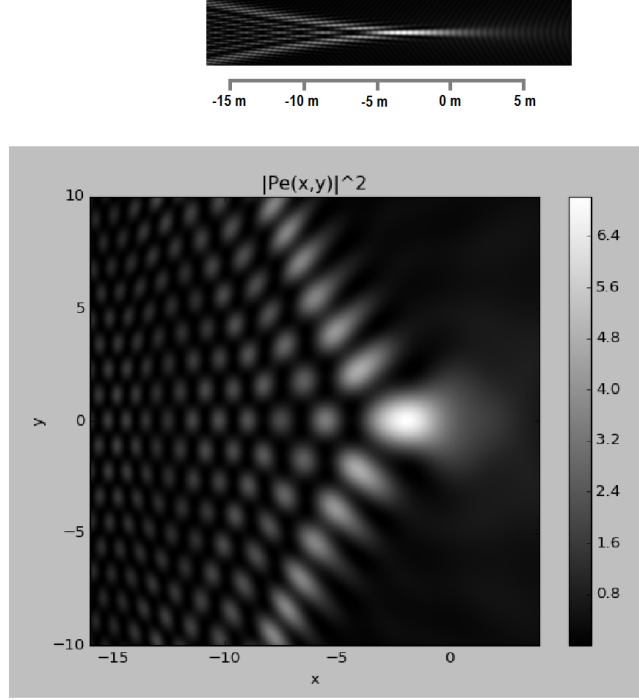


Figure 4: Top: Normalized near-cusp PSF obtained by numerical integration of (27, 28) for  $\beta = \pi/2$ ,  $\lambda = 10^{-6}\text{m}$  at 550AU (the whole caustic transversal size is about 500 meters), the aspect ratio is preserved. Bottom: Square of absolute value of the Pearcey integral.

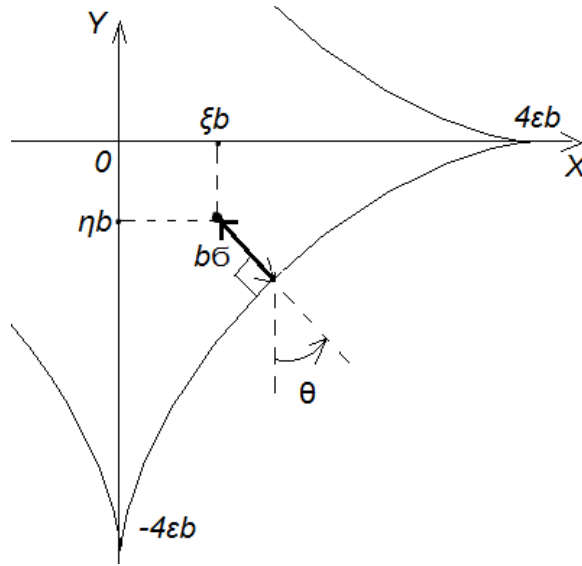


Figure 5: Correspondence between the Cartesian and caustic linked coordinates in the observer plane



we rewrite (45) as

$$F = \frac{1}{2\pi(3\epsilon q \sin 2\theta)^{1/3}} \int_{-(3\epsilon q \sin 2\theta)^{1/3}\pi}^{(3\epsilon q \sin 2\theta)^{1/3}\pi} e^{iV} d\varphi, \quad V = \tilde{\sigma}\varphi + \frac{1}{3}\varphi^3 + \tilde{W}, \quad (46)$$

where

$$\tilde{W} = \frac{\varphi^3}{(3\epsilon q \sin 2\theta)^{1/3}} \left[ \frac{\tilde{\sigma}\tilde{W}_1 + \varphi^2\tilde{W}_2}{(3\epsilon q \sin 2\theta)^{1/3}} + \varphi\tilde{W}_3 \cot 2\theta \right].$$

In the above equation  $\tilde{W}_1, \tilde{W}_2, \tilde{W}_3$  are bounded functions ( $\max(|\tilde{W}_1|, |\tilde{W}_2|, |\tilde{W}_3|) \leq 21/20$ ) of the single variable  $\phi = \frac{\varphi}{(3\epsilon q \sin 2\theta)^{1/3}}, \phi = -\pi \dots \pi$

$$\tilde{W}_1 = \frac{\sin \phi - \phi}{\phi^3}, \quad \tilde{W}_2 = 2 \frac{\sin \phi - \phi + \frac{\phi^3}{6} - 2 \sin 2\phi + 4\phi - \frac{(2\phi)^3}{3}}{\phi^5}, \quad \tilde{W}_3 = \frac{\cos 2\phi - 4 \cos \phi + 3}{\phi^4}.$$

When the conditions

$$|\tilde{\sigma}| \ll (\epsilon q \sin 2\theta)^{2/3}, \quad |\sin 2\theta| \gg \frac{1}{(\epsilon q)^{1/4}}, \quad q\epsilon \gg 1 \quad (47)$$

hold, the  $\tilde{W}$ -term can be neglected in (46), since  $\epsilon q \gg 1$ . Therefore

$$F = \frac{1}{2\pi(3\epsilon q \sin 2\theta)^{1/3}} \int_{-\infty}^{\infty} \exp i \left[ \tilde{\sigma}\varphi + \frac{\varphi^3}{3} \right] d\varphi = \frac{\text{Ai}(\tilde{\sigma})}{(3\epsilon q \sin 2\theta)^{1/3}},$$

where  $\text{Ai}(\tilde{\sigma})$  is the Airy function. Finally we get

$$\frac{\mu}{\mu_0} = \frac{1}{(3\epsilon q \sin 2\theta)^{2/3}} \text{Ai}^2 \left( \frac{-\sigma q}{(3\epsilon q \sin 2\theta)^{1/3}} \right), \quad |\sigma| \ll \epsilon |\sin 2\theta|, \quad |\sin 2\theta| \gg \frac{1}{(\epsilon q)^{1/4}}.$$

In terms of the unscaled distance from the caustic fold  $\mathcal{D} = \sigma b, b = \sqrt{2r_g Z}$  (see Figure 5)

$$\mu = \frac{4\pi^2 r_g}{\lambda K^2} \text{Ai}^2 \left( \frac{-2\pi \mathcal{D}}{K\lambda} \sqrt{\frac{2r_g}{Z}} \right), \quad K = \left( \frac{12\pi \epsilon r_g}{\lambda} \sin 2\theta \right)^{1/3}. \quad (48)$$

The validity domain of (48)

$$|\mathcal{D}| \ll b\epsilon |\sin 2\theta|, \quad |\sin 2\theta| \gg \frac{1}{(\epsilon q)^{1/4}} \quad (49)$$

is obviously contained in (35). The maximum of  $\text{Ai}(\tilde{\sigma})$  is reached at  $\tilde{\sigma} = -1.02$ , which satisfies (47). The diffraction pattern in the fold neighborhood, far from the cusps, is locally one dimensional with the oscillation scale  $\sim \lambda |3\epsilon q \sin 2\theta|^{1/3} / \alpha_E$  depending on the fold coordinate  $\theta$ . Also for maximal magnification at fixed  $\theta$  we have

$$\frac{\max_{\mathcal{D}} \mu(\mathcal{D}, \theta)}{\mu_0} = \frac{\max \text{Ai}^2}{(3\epsilon q \sin 2\theta)^{2/3}} \approx \frac{0.29}{(3\epsilon q \sin 2\theta)^{2/3}}, \quad \frac{\max_{\mathcal{D}} \mu(\mathcal{D}, \theta)}{\mu_{\epsilon}} \approx \frac{0.56}{(\epsilon q)^{1/6} \sin^{2/3} 2\theta}.$$

Taking into account that (48) is valid for  $|\theta| \gg (\epsilon q)^{-1/4}$  and  $\epsilon q \gg 1$ , we conclude that

$$\max_{\theta, \mathcal{D}} \mu(\mathcal{D}, \theta) < \mu_{\epsilon}.$$

This confirms an obvious fact that in a neighborhood of folds the intensity is smaller than the maximum  $\mu_\epsilon$  in the cusp region.

According to (41, 48) the GPSF oscillates and amplitude of oscillations falls as one moves away from the caustic and the "far field" GPSF can be approximated by (17).

**3.** Concluding this section we mention the case when the observer is on the  $z$ -axis, i.e. when  $X = Y = 0$ : Here, the integral (34) is expressed in terms of the zero-order Bessel function and

$$\mu_{\text{axis}} = \pi q J_0^2(\epsilon q), \quad \frac{\mu_{\text{axis}}}{\mu_0} = J_0^2(\epsilon q). \quad (50)$$

When  $\epsilon q \gg 1$ , i.e. when the size of the caustic exceeds greatly the diffraction radius<sup>13</sup>

$$\frac{\mu_{\text{axis}}}{\mu_0} = \frac{2}{\epsilon q} \cos(\epsilon q - \pi/4), \quad \epsilon q \gg 1$$

which is in agreement with (17).

## 5 Discussion and Conclusions

From the above it follows that the transversal size of the astroid caustic (due to the quadrupole moment of the sun) could reach several hundred meters at the distance of the closest observation. This size is comparable with sizes of images of possible objects of observation, which are about several kilometers across. The diffraction pattern of a point source in the sub-micrometer diapason of the EM spectrum transforms significantly when the direction of observation is changed from the one along the sun polar axis to that in the sun equatorial plane. The maximum of the point spread function can differ up to about two-three orders of magnitude.

We recall that the maximum of PSF is the maximal magnification of the point source. The maximal magnification of a realistic extended object depends on its size. For example, magnification of exo-planets to be observed with the solar gravitation lens is determined mainly by the geometrical optics. In this case, the wave-optics effects, like change of the maximum of PSF, are invisible without a fine-scale very high resolution de-convolution of the object's image. However, change of geometrical optics magnification due to presence of a caustic can be observed at much rougher resolution of de-convolution.

We also note that, even for a point source, the GPSF (27, 28) is, in fact, a point spread function for a "zero-aperture" telescope. For realistic apertures one should use the PSF of a compound system of the gravitational lens and a telescope (for more details see eg [21]). In the Fraunhofer approximation for the telescope lens of the focal length  $\mathcal{F}$ , the PSF in the telescope focal plane reads as

$$\mathcal{M}(\vec{\gamma}; \vec{\omega}) = |w(\vec{\gamma}; \vec{\omega})|^2, \quad w(\vec{\gamma}; \vec{\omega}) = \frac{k}{2\pi i \mathcal{F}} \int_{\vec{R} \in \text{Aperture}} u(\vec{R} - \vec{\omega} Z) e^{ik(\vec{\omega} + \vec{\gamma})\vec{R}} d^2 R,$$

where  $\vec{\gamma}$  and  $\vec{\omega}$  are the observation and the point source angles correspondingly, and  $\vec{R} = (X, Y)$  are coordinates in the aperture (observer) plane. The complex amplitude of the EM field at the aperture plane  $u(\vec{R} - \vec{\omega} Z) e^{ik\vec{\omega}\vec{R}}$  is expressed through  $u(\vec{R})$  given by (16).

---

<sup>13</sup>i.e. when an on-axis observer sees the perfect "Einstein cross" image in the lens plane.

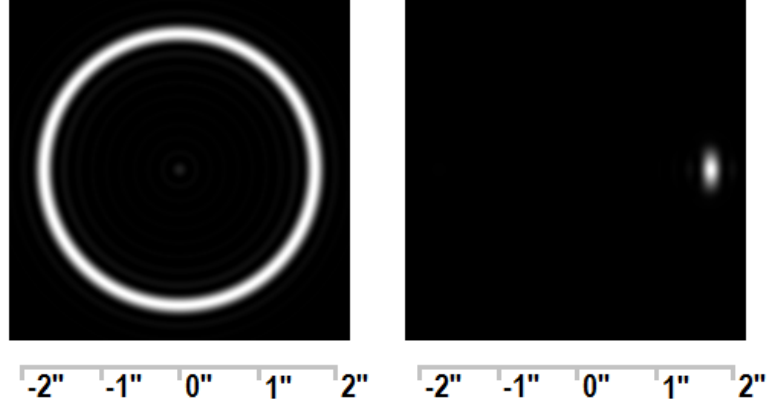


Figure 6: Focal plane PSF for 1-meter telescope ( $a = 0.5\text{m}$ ) for  $\lambda \approx 10^{-6}\text{m}$  at 550 AU. Left: Symmetric  $\epsilon = 0$  case. Both telescope and source are placed on the polar axis  $\beta = 0$ ,  $X = Y = 0$ . Right: Observation in the equatorial plane  $\beta = \pi/2$ ,  $\epsilon \approx 10^{-7}$ . Telescope is placed at the cusp vertex  $X = 4\epsilon b$ ,  $Y = 0$ . The maximum of the "equatorial" PSF (right) exceeds that of the  $\epsilon = 0$  "polar axis" PSF (left) by  $\approx 1.2$  times.

Similarly to the case of the GPSF (27, 45), the above focal plane PSF easily reduces to one-dimensional integral in  $\phi$  by the stationary phase method. When (35) holds

$$\mathcal{M} = \mu_0 \left( \frac{ka^2}{2\mathcal{F}} \right)^2 |F|^2, \quad F = \frac{1}{\pi} \int_0^{2\pi} e^{ik\alpha_E(eb \cos 2\phi - X \cos \phi - Y \sin \phi)} h\left(ka\alpha_E \left| e^{i\phi} - \Gamma e^{i\theta} \right| \right) d\phi,$$

where  $a$  is the radius of aperture and  $h(x) = J_1(x)/x$ , with  $J_1$  standing for the first-order Bessel function. Here  $\Gamma, \theta$  are the dimensionless polar coordinates in the focal plane and  $X, Y$  denote deviation from the line that passes through the point source and the sun center

$$\vec{\gamma} = (\alpha_E \Gamma \cos \theta, \alpha_E \Gamma \sin \theta), \quad (X, Y) = -\vec{\omega} Z$$

For very big realistic apertures and very small source angles (i.e. for  $a\alpha_E \gg \lambda$  and  $a|\vec{\omega}| \ll \lambda$ ) this function is "concentrated", within the telescope diffraction limit, around the Einstein ring  $\Gamma = 1$ .

It is important to note that, in difference from the GPSF  $\mu$ , the maximum of the focal plane PSF  $\mathcal{M}$  is not necessarily smaller for equatorial observations in comparison with polar observations, when the aperture is big enough (see Figure 6).

Most likely, in a possible mission, a sequence of images of the Einstein rings along a path of a spacecraft across the source image will be taken. The intensity of a ring point in this set, in a sense, encodes "projection data" taken along a "section" of the source surface. Therefore, a kind of "tomographic" reconstruction algorithms should be developed for the de-convolution related with the above PSF.

Finally, we would like to mention the influence of the higher multi-pole moments of the sun on the PSF. Computation of the PSF accounting for higher moments is a straightforward generalisation of the case considered in this work: one should add the higher-order harmonic terms to the potential  $\psi$  in (8)

$$\psi = \text{Re} \left[ \log(\zeta) - \sum_{n=2}^{\infty} \epsilon_n \zeta^{-n} \right], \quad \zeta = \rho e^{i\phi},$$

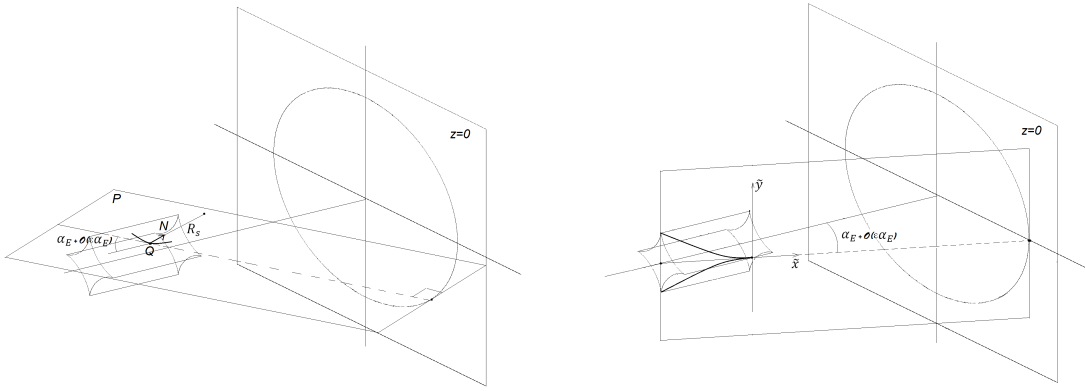


Figure 7: Left: Section of the caustic at fold ( $N$  is vector normal to the caustic at  $Q$ ). Right: Section of the caustic at cusp.

where  $\epsilon_n$  are complex harmonic moments. Then one could perform the geometric optics analysis and the stationary phase integration with an account of a new potential.

## 6 Appendix 1

Below we perform the double check of our main results for the strongly non degenerate case  $q\epsilon \gg 1$  ( $\epsilon \gg \lambda/r_g$ ) using algorithms from the geometrical diffraction theory.

We start with the computation of the intensity near a regular point of the caustic. According to the theory of the uniform (caustic) expansions, the intensity magnification in vicinity of a regular point  $Q$  of the caustic surface equals to (see e.g. [13], [17])

$$\mu = 2\pi U \left( \frac{2k^2}{R_s} \right)^{1/6} \text{Ai}^2 \left( -\mathcal{D} \sqrt[3]{\frac{2k^2}{R_s}} \right), \quad (51)$$

where  $\mathcal{D}$  is the distance to the caustic from its convex side. Here,  $R_s$  stands for the radius of curvature of section of the caustic surface by the plane  $P$  containing the tangent at  $Q$  light ray. The plane  $P$  also contains the vector normal to the caustic at  $Q$  (see Figure 7). The pre-factor  $U = U(Q)$  in (51) is determined by matching the geometrical optics value of magnification (11) in vicinity of the caustic (taking into account the multiplicity of images) with the following asymptotics of (51) at  $\mathcal{D} \gg (R_s/k^2)^{1/3}$

$$\mu \rightarrow \frac{U}{\sqrt{\mathcal{D}}}. \quad (52)$$

To find all the above values, we use the expansion in the proximity of the critical line (12)

$$\rho = \rho_c(\theta) + \Delta\rho. \quad (53)$$

It is now convenient to introduce another set of the caustic-linked coordinates  $\Delta\rho, \theta$  (also see eq. (13))

$$(X, Y) = (b\xi_c(\theta), b\eta_c(\theta)) + \Delta\vec{r}, \quad \Delta\vec{r} = (2b\Delta\rho \cos \theta, 2b\Delta\rho \sin \theta). \quad (54)$$

Vector  $\Delta\vec{r}$  is tangent to the caustic at  $Q$ . Therefore, for small  $\Delta\vec{r}$ , the distance from the caustic to the point  $(X, Y, Z)$  equals

$$\mathcal{D} = \frac{\Delta\vec{r}^2}{2R_a} = \frac{2b^2}{R_a}\Delta\rho^2,$$

where  $R_a$  is the radius of curvature of the astroid (13)

$$R_a = 6b\epsilon \sin(2\theta).$$

The point  $(X, Y)$  has two ("strong") pre-images in the close vicinity of the critical line <sup>14</sup> with

$$\Delta\rho = \pm \frac{1}{2b} \sqrt{2R_a \mathcal{D}}.$$

On the other hand, it follows from (53) and (11) that away from the caustic  $\mu = \frac{1}{4\Delta\rho}$  and with account of image multiplicity and signs we get

$$\mu = \frac{1}{2|\Delta\rho|} = \frac{b}{\sqrt{2R_a \mathcal{D}}}.$$

Comparing the above equation with (52) we get

$$U = b/\sqrt{2R_a} = b/\sqrt{12\epsilon b \sin 2\theta}.$$

Also

$$R_s = R_a/\alpha_E^2 = \frac{6\epsilon b \sin(2\theta)}{\alpha_E^2},$$

since the plane  $P$  intersects the  $z$ -axis under the angle  $\alpha_E + \mathcal{O}(\alpha_E \epsilon)$  (see Figure 7).

Plugging the above values of  $U$  and  $R_s$  into (51), with the help of (6, 15), we get the expected final expression (48) for the near-fold GPSF.

Let us now consider the pattern in regions near the turning points  $\theta = 0, \pi/2, \pi, 3\pi/2$ , where intensity reaches its maximum. Without loss of generality we take the cusp at  $\theta = 0$ .

According to the theory of the uniform caustic expansions (see eg [17], [20]), in the local coordinates of the section plane  $\tilde{x}, \tilde{y}$  (see Figure 7), where equation of the caustic has the approximate form

$$\tilde{x}^3 = -\frac{9}{8}a\tilde{y}^2, \tag{55}$$

the magnification equals

$$\mu(\tilde{x}, \tilde{y}) = W \left| \text{Pe} \left( \tilde{x} \left( \frac{6k}{a} \right)^{1/2}, \tilde{y} \left( \frac{24k^3}{a} \right)^{1/4} \right) \right|^2. \tag{56}$$

Here, the pre-factor  $W$  is determined by matching the geometrical optics value of magnification (11) in the cusp neighborhood with the corresponding asymptotics of (56). It is convenient to set  $\tilde{y} = 0$  and use the asymptotics of (56) for  $\tilde{x} \gg \sqrt{\frac{a}{6k}}$

$$\mu(\tilde{x}, 0) \rightarrow \frac{\pi W}{\tilde{x}} \sqrt{\frac{a}{6k}}. \tag{57}$$

---

<sup>14</sup>and up to four pre-images in total, depending on the observer position relatively to the caustic.

The section plane is parallel to the  $y$ -axis and intersects the  $z$ -axis under the angle  $\alpha_E + \mathcal{O}(\alpha_E \epsilon)$  (see Figure 7). Therefore

$$\tilde{X} = \alpha_E \tilde{x}, \quad \tilde{Y} = \tilde{y}, \quad (58)$$

where  $(\tilde{X}, \tilde{Y})$  is the deviation from the cusp vertex in the observer  $z = Z$  plane. Taking (58) into account, from (55) and (13) we get

$$a = 12\epsilon b / \alpha_E^3.$$

From (11) it follows that for  $\tilde{Y} = 0$  and  $\tilde{X} > 0$ , near the cusp  $\mu \rightarrow \frac{b}{2\tilde{X}}$ . Then with the help of (57, 58) we obtain

$$W = \frac{1}{4\pi} \sqrt{\frac{2kb\alpha_E}{\epsilon}}.$$

Substituting the above values in (56) and taking (58) into account we get the expected expression (41) for the near-cusp GPSF.

## References

- [1] Eshleman, Von R., *Gravitational lens of the sun: its potential for observations and communications over interstellar distances*, Science, Vol. 205, no. 4411 (1979) pp. 1133-1135.
- [2] V.R.Eshleman, G.L.Tyler, W.T.Freeman, *Deep radio occultations and evolute flashes; their characteristics and utility for planetary studies*, Icarus, Volume 37, Issue 3, March 1979, Pages 612-626
- [3] Geoffrey A. Landis, *Mission to the Gravitational Focus of the Sun: A Critical Analysis*, 55th AIAA Aerospace Sciences Meeting, AIAA SciTech Forum, (AIAA 2017-1679), <https://arxiv.org/ftp/arxiv/papers/1604/1604.06351.pdf>
- [4] S.G. Turyshev, B-G Andersson, *The 550 AU Mission: A Critical Discussion*, Mon. Not. Roy. Astron. Soc. 341 (2003) 577-582
- [5] Claudio Maccone, *Deep Space Flight and Communications: Exploiting the Sun as a Gravitational Lens*, Springer Science and Business Media, 2009 - 402 pages
- [6] R. Epstein and I. Shapiro, *Post-Post-Newtonian Deflection of Light by the Sun*, Phys. Rev. D, 22, 1980
- [7] Laurent Koechlin, Denis Serre, Gerald K. Skinner, Peter Von Ballmoos, Thomas Crouzil, *Multiwavelength focusing with the Sun as gravitational lens*, Exp Astron (2005) 20:307315
- [8] E. Herlt and H. Stephani, *Wave optics of the spherical gravitational lens part I: Diffraction of a plane electromagnetic wave by a large star*, Int. J. Theor. Phys. 12, 81 (1975)
- [9] E. Herlt and H. Stephani, *Wave optics of the spherical gravitational lens. II. Diffraction of a plane electromagnetic wave by a black hole*, Int. J. Theor. Phys. 15, 45 (1976)
- [10] S.G.Turyshev, *Wave-theoretical description of the solar gravitational lens*, Phys. Rev. D 95, 084041 (2017)

- [11] Slava G. Turyshev, Viktor T. Toth, *Diffraction of electromagnetic waves in the gravitational field of the Sun*, Phys. Rev. D 96, 024008 (2017)
- [12] P.Schneider, J.Ehlersand, E.E.Falco, *Gravitational Lenses*, (Springer-Verlag, Berlin, 1992)
- [13] Landau L. D.; Lifshitz E. M, *The classical theory of fields*, Oxford: Pergamon Press, 1975
- [14] Mauro Sereno, *Gravitational Faraday rotation in a weak gravitational field*, Phys.Rev. D 69 (2004) 087501
- [15] Mauro Sereno, *Gravitational lensing in metric theories of gravity*, Phys. Rev. D 67, (2003) 064007
- [16] Hideki Asada, Masumi Kasai, *Can we see a rotating gravitational lens?*, Prog.Theor.Phys. 104 (2000) 95-102
- [17] V. A. Borovikov, B. E. Kinber, *Geometrical Theory of Diffraction*, IEE electromagnetic waves series N37, 1994
- [18] Sergei Kopeikin, Bahram Mashhoon, *Gravitomagnetic Effects in the Propagation of Electromagnetic Waves in Variable Gravitational Fields of Arbitrary-Moving and Spinning Bodies*, Phys.Rev.D 65:064025, 2002
- [19] Takahiro T. Nakamura and Shuji Deguchi, *Wave Optics in Gravitational Lensing*, Progress of Theoretical Physics Supplement No. 133, 1999
- [20] Pearcey T., *The Structure of Electromagnetic Field in the Neiborhood of a Cusp of a Caustic*, Phyl. Mag., 1946, v. 37, p. 311
- [21] Yasusada Nambu, *Wave optics and image formation in gravitational lensing*, Journal of Physics: Conference Series, Volume 410, conference 1, 2013